RSC Pharmaceutics

ROYAL SOCIETY OF CHEMISTRY

PAPER

View Article Online
View Journal | View Issue

Check for updates

Cite this: *RSC Pharm.*, 2025, **2**, 1593

Aluminium-complexed alginate nanoparticles as an adjuvant for therapeutic vaccines against melanoma

Meera Menon TP, Anjana Unnikrishnan, Reba Elsa Sam, Mohammed Ashif, Jisnet George, Bins KC, Unnikrishnan Sivan, Ajith Vengellur and Anusha Ashokan *

Therapeutic cancer vaccines elicit an immune response within existing tumours. Our research introduces a strategy to address the low efficacy of peptide-based therapeutic cancer vaccines by employing aluminum-complexed alginate nanoparticles (nAl-Alg) as an adjuvant. Characterisation of nAl-Alg revealed a hydrodynamic diameter of 242.1 ± 126.33 nm. Cytocompatibility studies using the murine macrophage cell line RAW 264.7 demonstrated no change in percentage viability up to 100 μg ml^{-1} compared to the untreated control. Cell uptake studies conducted in RAW 264.7 macrophages demonstrated an enhanced uptake of nAl-Alg compared to Alhydrogel®, a commercially available adjuvant. *In vivo* toxicity studies in mouse models also revealed the absence of adverse reactions in haematological analysis after treatment with nAl-Alg. Subsequent *in vivo* mouse melanoma model studies showed a notable delay in tumour growth in animals treated with nAl-Alg combined with the tumour antigen compared to groups treated with the tumour antigen alone, adjuvant alone, and untreated controls. The median survival time increased from 17 days in untreated animals to 33 days for the nAl-Alg and tumour antigen combination-treated group. Treatment with nAl-Alg and the tumour antigen alone resulted in median survival times of 23 days and 24 days, respectively. These findings highlight the potential therapeutic impact of nAl-Alg in enhancing the immune response against tumours.

Received 21st April 2025,
Accepted 11th September 2025

DOI: 10.1039/d5pm00111k

rsc.li/RSCPharma

Open Access Article. Published on 19 September 2025. Downloaded on 4/28/2026 7:03:43 AM.
This article is licensed under a Creative Commons Attribution 3.0 Unported Licence.

1. Introduction

Therapeutic cancer vaccines (TCVs) are a promising approach to cancer treatment, designed to target and destroy malignant tumours present in the body with minimal effects on other tissues.[1,2] TCVs primarily focus on tumour-specific cellular immune responses crucial for directly eliminating cancer cells.[2,3] They are categorised mainly into cell-based, virus-based, peptide-based, and nucleic acid-based vaccines.[4] They hold promise, but these vaccines encounter drawbacks such as limited T-cell responses and the risk of antigen evasion.[5,6]

Researchers are exploring novel approaches to address these challenges, such as incorporating advanced adjuvants to enhance antigen presentation and stimulate anti-tumour T-cell response.[7,8] The use of adjuvants, including nanomaterials, has been explored to enhance the immune response to antigens.[7,9] The traditional adjuvants used in TCVs include alum and lipid-based adjuvants. Alum adjuvants, commonly used in vaccines, have been shown to induce innate immune pathways, producing cytokines such as IL-1β and Th2-type immune responses.[10] However, alum adjuvants fail to induce strong Th1-type and cellular immune responses that have been shown to enhance anti-tumour immunity.[11,12] Therefore, the use of alum adjuvants in therapeutic cancer vaccines is limited.[13] Liposome-based adjuvants are a promising strategy to stimulate Th1-biased immune responses.[8,14,15] However, the manufacturing techniques for liposomal adjuvants are labour-intensive, need better reproducibility, and may need to be more cost-effective. These challenges can impact the scalability and commercial viability of lipid-based adjuvants.[16,17]

Nanoparticle-based formulations offer unique advantages for enhancing vaccine efficacy. Nanoparticles have a high surface area-to-volume ratio compared to larger particles, making them efficient delivery vehicles for antigens.[18,19] The smaller size of the nanoparticles facilitates improved trafficking to lymph nodes and enhanced uptake by antigen presenting cells.[20–22] Furthermore, nanomaterials promote cross-presentation of antigens to cytotoxic T lymphocytes (CTLs) which is critical for therapeutic cancer vaccine development.[23] Aluminium based nanoparticles have shown promise in enhancing anti-tumour immune responses by promoting the activation and proliferation of CTLs.[24] Unlike conventional

Department of Biotechnology, Cochin University of Science and Technology, Kerala, India. E-mail: anusha.ashokan@gmail.com

© 2025 The Author(s). Published by the Royal Society of Chemistry

Open Access Article. Published on 19 September 2025. Downloaded on 4/28/2026 7:03:43 AM. This article is licensed under a Creative Commons Attribution 3.0 Unported Licence.

alum adjuvants, nano-alum exhibits superior immunostimulatory properties and has been shown to improve cytotoxicity against cancer cells in preclinical studies.[25] Furthermore, recent research by Mark T. Orr *et al.* has revealed the efficacy of nano-alum in eliciting Th1 immune responses, which include the production of pro-inflammatory cytokines like interferon-gamma (IFN-γ) and tumour necrosis factor (TNF), which are critical for anti-tumour immunity.[26] Given the limited biodegradability of alum-based materials,[27] we investigated the adjuvant properties of a polymer-based formulation incorporating aluminium. Alginate was chosen as the polymer due to its biocompatibility, biodegradability, and potential adjuvant properties.[28,29] A previous study demonstrated that combining alginate with the BCG vaccine as an adjuvant significantly enhanced the immune response in mice, as evidenced by increased IFN-gamma and immunoglobulin production.[29]

In this study, our primary objective was to design and evaluate aluminium-complexed alginate nanoparticles (nAl-Alg) as potential adjuvants for TCVs. We conducted cytocompatibility and *in vivo* toxicity studies to assess the safety profile of these nano-adjuvants. Furthermore, we investigated the efficacy of these adjuvants through *in vivo* anti-tumour experiments utilising tumour lysate as the antigen source.

2. Materials and methods

2.1. Materials

Alginic acid sodium salt from brown algae with low viscosity (A0682) and aluminium chloride hexahydrate ($AlCl_3{\cdot}6H_2O$, 237078, CAS Number 7784-13-6) were procured from Sigma-Aldrich. The B16-F10 murine melanoma cell line and RAW 264.7 murine macrophage cell line were purchased from the National Centre for Cell Science, Pune, India, and were used for *in vitro* and *in vivo* studies. B16-F10 and RAW 264.7 cell lines were cultured in Dulbecco's modified Eagle's medium with high glucose (AL007-Himedia), supplemented with 10% fetal bovine serum (10270106-Gibco™) and 1% penicillin–streptomycin solution (P4333-Sigma-Aldrich). Bicinchoninic acid (Sigma Aldrich, reagent A # B9643, reagent B #C2284) and 3-(4,5-dimethylthiazol-2-yl)-2,5-diphenyltetrazolium bromide (MTT, Invitrogen™) were purchased for protein estimation and cytocompatibility analysis. Lumogallion (TCI, CAS RN 4386-25-8, A5060), 4′,6-diamidino-2-phenylindole (DAPI) (HiMedia PCT1539), piperazine-*N*,*N*′-bis(2-ethanesulfonic acid) (PIPES) buffer (HiMedia RM659), Alhydrogel® adjuvant 2% (InvivoGen, CAS number: 21645-51-2), paraformaldehyde (HiMedia, TCL119), and Fluoroshield™ (Sigma Aldrich, F6182) were also used.

2.2. Animals

C57BL/6 mice aged 4–8 weeks were acquired from the Division of Laboratory Animal Science, Sree Chitra Tirunal Institute of Medical Science and Technology, Trivandrum. All animals were housed at the Small Animal Facility of the Cochin University of Science and Technology. All animal procedures were performed in accordance with the Guidelines for Care and Use of Laboratory Animals of Cochin University of Science and Technology and approved by the Animal Ethics Committee of the Cochin University of Science and Technology.

2.3. Synthesis and characterization of nAl-Alg

nAl-Alg was synthesised by dropwise addition of 0.9 mM $AlCl_3{\cdot}6H_2O$ to an equal volume of 0.3% (w/v) sodium alginate solution placed on a magnetic stirrer at room temperature (24–26 °C). The solution was agitated for 15 min. The mixture was then transferred to a centrifuge tube and centrifuged at 19 000 rpm in a WX ULTRA 100 centrifuge for 30 min at 4 °C. The supernatant liquid was collected, and the pellet was resuspended with 5 ml Milli-Q water. This washing process was repeated thrice. The pellet was finally dispersed in 2–5 ml Milli-Q water and stored at 4 °C.

Inductively coupled plasma mass spectrometry (ICP-MS). ICP-MS analysis was carried out to determine the percentage incorporation of aluminium into nAl-Alg. 10 ml of the supernatant liquid collected during synthesis and washing steps was analysed using a Thermo Fisher Scientific iCAP RQ.

Field emission scanning electron microscopy (FE-SEM). For FE-SEM analysis, the sample was diluted to 2 μg ml^{-1} after sonication and spotted on a metallic foil for air drying. The sample was mounted onto a stub and gold sputtered. The images were taken using a Field Emission Scanning Microscope, Zeiss Sigma.

Dynamic light scattering (DLS). The size distribution of nAl-Alg was assessed using Anton Paar Litesizer. Sonicated samples were diluted using Milli-Q water, and the instrument's protocol was followed for analysis. For reliability, each experimental procedure was conducted in triplicate. Probe sonication was avoided on day 15 and day 55 for stability analysis.

Energy dispersive X-ray (EDX) analysis. Elemental analysis was performed using an Oxford XMX N. Approximately 1–2 mg of dried nAl-Alg sample was affixed to the holder, consisting of adhesive carbon tape secured onto a brass stub. This assembly was inserted into the scanning electron microscope chamber. The working voltage was adjusted to 20 keV for sample analysis.

Fourier transform infrared (FTIR) spectroscopy. FTIR spectroscopic analysis was conducted using a Thermo Nicolet iS50 FTIR spectrophotometer with a resolution of 0.2 cm^{-1}. Dried and powdered nAl-Alg were examined using a KBr window. KBr-sample pellets were prepared, and 32 scans per sample were taken within the 400 to 4000 cm^{-1} spectral range. Initial background spectra were collected, and atmospheric corrections were applied using software.

Solid-state nuclear magnetic resonance (ssNMR) spectroscopy. Magic Angle Spinning NMR (MAS-NMR) spectra were acquired on an ECZR Series 500 MHz NMR spectrometer equipped with a 3.2 mm HXMAS probe capable of high-speed magic-angle spinning (MAS) up to 20 kHz. A finely powdered adamantane ($C_{10}H_{16}$) sample (used as the chemical shift refer-

© 2025 The Author(s). Published by the Royal Society of Chemistry

Open Access Article. Published on 19 September 2025. Downloaded on 4/28/2026 7:03:43 AM. This article is licensed under a Creative Commons Attribution 3.0 Unported Licence.

ence standard), weighing approximately 10–15 mg, was packed into a 1 mm rotor and inserted into the stator of the solid-state probe. After calibration, adamantane was removed from the probe, and the sample to be analyzed (nAl-Alg/sodium alginate) was inserted. To record the ^{1}H NMR spectrum, a single-pulse experiment was employed with 256 scans and a 5-second relaxation delay, while maintaining a spinning speed of 6 kHz. For ^{13}C spectra, a cross-polarization MAS experiment with a spinning speed of 10 kHz was conducted, utilizing 1024 scans and a 5-second relaxation delay. Sodium (^{23}Na) spectra were acquired with 512 scans, a 3-second relaxation delay, and a spinning speed of 10 kHz. Finally, aluminum (^{27}Al) spectra were obtained with 512 scans, a 1.5-second relaxation delay, and a spinning speed of 10 kHz.

2.4. Bacterial endotoxin test of nAl-Alg

An E-TOXATE™ kit (Sigma) was used to detect bacterial endotoxins in nAl-Alg, with a sensitivity limit of 0.05–0.1 endotoxin units (EU) per mL. The provided kit contained E-TOXATE™ Reagent, E-TOXATE™ endotoxin standard (*Escherichia coli* O55:B5 lipopolysaccharide) and endotoxin-free water. All the procedures were followed as per the manufacturer's manual. The testing procedure involved labelling four tubes as follows: tube A – nAl-Alg, tube B – nAl-Alg + endotoxin standard, tube C – endotoxin free water (negative control), and tube D – endotoxin standard (positive control). 100 μl of test solutions were added to the tubes, followed by E-TOXATE™ Reagent Working Solution (100 μl). After gentle mixing, the tubes were covered and incubated at 37 °C for 1 hour. Following incubation, each tube was inverted to check for gelation. A hard gel indicates a positive test for endotoxin, while soft gels, turbidity, or clear liquids are considered negative. A clot in the inhibitor tube B shows that no inhibitor is present in nAl-Alg.

2.5. Cytocompatibility analysis of nAl-Alg

Cytocompatibility analysis was performed by MTT assay on RAW 264.7 macrophages. RAW 264.7 cells (1×10^4 cells per well) were seeded into a 24-well plate and incubated for 12 hours in DMEM containing 10% FBS and 1% penicillin/streptomycin. Varying concentrations of nAl-Alg (10–200 μg ml^{-1}) were added to the cells and then they were incubated for 48 hours. After incubation, the MTT reagent was added, followed by the addition of DMSO to dissolve the formazan crystals. The absorbance was measured at 570 nm in a Tecan Spark multimode plate reader. The data from the MTT cytotoxicity assay were obtained from three independent experiments, each comprising three replicates (n = 9).

2.6. Evaluation of nAl-Alg cellular uptake by lumogallion staining

Cellular uptake of nAl-Alg was investigated and compared with Alhydrogel®, a commercially available adjuvant. RAW 264.7 cells (2×10^4) were seeded onto coverslips in a 24-well plate. After 24 hours, the cells were observed and treated with 50 μg of nAl-Alg and 5 μL (~50 μg Al) of Alhydrogel. After 3 hours, all media were removed, and the cells were washed with 50 mM 2,2′-piperazine-1,4-diylbisethanesulfonic acid (PIPES) buffer three times. Subsequently, 250 μl of paraformaldehyde (PFA) was added to each well, covered with aluminum foil, and left at room temperature for 20 minutes. The PFA was then removed, and the cells were rewashed with PIPES buffer thrice for 5 minutes each. The cells were stained with 50 μM lumogallion (TCI, A5060) in 50 mM PIPES buffer and incubated at room temperature for 30 minutes. After incubation, the cells were washed with PIPES buffer thrice for 5 minutes each. A 1 : 500 DAPI solution in 1× PBS was prepared and added to each well, followed by a 20-minute incubation at room temperature. The cells were washed with 1× PBS thrice for 5 minutes each. The slides were labelled with each group, and 10 μl of FluoroShield™ (Sigma-Aldrich, F6182) was added to each slide. The coverslips were carefully removed from the wells and placed inverted on the slides (cell side facing the FluoroShield™). After drying, the edges were sealed with colorless enamel paint. Cell images were captured at 20× and 60× (oil immersion) magnifications using a Nikon Eclipse Ti2 inverted fluorescent microscope. Lumogallion analysis used fixed exposure settings of 100 ms and DAPI at 20 ms in all images, with preset light transmission values. Images were captured and analyzed, and fluorescence and light channels were overlaid using Nikon NIS Elements software. The mean fluorescence intensity (MFI) of 100 cells in each group (n = 100) was quantified using ImageJ software.

2.7. *In vivo* toxicity studies

Toxicity studies were conducted on six C57BL/6 mice aged five weeks. The animals were randomly divided into two groups, each containing 3 animals (n = 3). They were subcutaneously injected with nAl-Alg (8.6 mg kg^{-1}) and saline on the left flank. The treatment was repeated on day five and day ten. On day 11, the animals were euthanised, and blood was collected by cardiac puncture. The collected blood was analysed for whole blood cell count and renal and hepatic function parameters.

2.8. *In vivo* tumour model study

The melanoma tumour model was developed following the protocol described in our previous work on therapeutic cancer vaccines.[30] Tumor induction was achieved by subcutaneous injection of 1×10^6 B16-F10 melanoma cells into the right flank of the animals. On day 5, the animals were divided into four groups, four animals per group (n = 4): (1) untreated control, (2) animals treated with B16-F10 melanoma cell lysate as the antigen, (3) animals treated with nAl-Alg alone (8.6 mg kg^{-1}), and (4) animals treated with a combination of B16-F10 cell lysate and nAl-Alg. The physical randomisation method was used to allocate animals to four different groups. B16-F10 melanoma cell lysate was prepared using the freeze–thaw method, and the protein estimation was done using BCA analysis.[30] Subcutaneous injection of the samples was administered to the left flank of the animals on days 5, 10, and 15 post-tumor induction. The concentration of nAl-Alg administered in both the adjuvant alone group and the adjuvant plus

© 2025 The Author(s). Published by the Royal Society of Chemistry

Open Access Article. Published on 19 September 2025. Downloaded on 4/28/2026 7:03:43 AM. This article is licensed under a Creative Commons Attribution 3.0 Unported Licence.

tumor lysate group was 8.6 mg kg^{-1}. A total volume of 100 μL of the sample was injected subcutaneously. Tumour measurements were taken from day five, once every 2–5 days, until the tumour volume reached 2 cm^3 using a vernier calliper. Animals were euthanized upon reaching the humane endpoint of a 2 cm^3 tumor volume. Tumours were subsequently collected.

2.9. Statistical analysis

Results are expressed as mean ± SEM. Data presentation and statistical analysis were performed using GraphPad Prism 8 software. Statistical significance was determined using one-way ANOVA (cell viability and cell uptake), Kaplan–Meier survival analysis (anti-tumor study) and Student's *t*-test (*in vivo* toxicity analysis). For one-way ANOVA, Dunnett's multiple comparison test (cell viability) and Tukey's multiple comparison test (cell uptake) were used as appropriate. The degree of significance is indicated by asterisks where appropriate: $*P < 0.05$ and $***P < 0.0005$ for Student's *t*-test. In ANOVA, significance was represented by $**P < 0.01$ and $****P < 0.0001$.

3. Results and discussion

3.1. Synthesis and characterization of nAl-Alg

Engineered nanomaterials with immunostimulatory properties hold great promise as adjuvants in therapeutic cancer vaccines. nAl-Alg was synthesised *via* the reaction of $AlCl_3{\cdot}6H_2O$ with linear copolymer sodium alginate. The concentration of the precursors was optimised to obtain nano-sized aluminium alginate particles. ICP-MS analysis of the supernatant liquid, collected during the synthesis of nAl-Alg, was carried out to quantify the percentage of Al^{3+} incorporation into the nAl-Alg complex. As shown in Fig. 1A, 44.7 ± 5.1% of Al^{3+} ions were complexed into nAl-Alg. The FE-SEM image of nAl-Alg (Fig. 1B) shows particles with an average particle size of ~114 nm. The hydrodynamic size of the nanoparticles was also assessed by DLS. The percentage intensity plot of redispersed nAl-Alg in Milli-Q water (Fig. 1C) showed an average hydrodynamic diameter of 242.5 ± 126.33 nm. The obtained PDI value of 0.19 showed that nAl-Alg has a relatively narrow size distribution. The stability of nAl-Alg on storage was studied by conducting a DLS analysis of the sample at three different time points (0^{th}, 15^{th}, and 55^{th} days). The intensity-weighted plots of nAl-Alg, Fig. 1D, showed an increase in the particle size diameter from 242.5 ± 126.33 nm on day 0 (the same data as Fig. 1C) to 299.8 ± 129.54 nm on day 55. The corresponding number weighted data presented in Fig. S1 (SI) demonstrate an increase in diameter from 82 ± 16 nm on day 0 to 156 ± 36 nm on day 55. The stability data showed no significant agglomeration of particles during the storage of nAl-Alg for 55 days. As observed, there is a significant difference in particle diameters mentioned from FE-SEM and intensity weighted DLS data. Previous studies have reported better correlation between particle sizes measured using electron microscopy and number weighted DLS data.[31] The broader size variation we observe in intensity weighted distribution compared to number weighted distribution might be due to the comparatively lower percentage of larger sized particles that contribute more significantly to intensity signals in DLS measurements.[31] Given the low PDI value of 0.19, the observed size distribution of the formulation is relatively narrow. Therefore, we anticipate that size heterogeneity will have minimal impact on the *in vitro* and *in vivo* responses of the nanomaterial. Considering the relevance of lyophilization for the long term storage of vaccines and improving the stability of the formulation, we lyophilized nAl-Alg using sucrose as the cryoprotectant. The control sample without cryoprotectant exhibited a larger mean particle size (336 ± 40 nm) and a PDI of 0.5 (Fig. S2). When an nAl-Alg to sucrose weight ratio of 1 : 1 was used, the size decreased to 219 ± 83 nm (PDI = 0.25). Further increasing the sucrose ratio to 1 : 20 reduced the mean size to 195 ± 75 nm and the PDI to 0.1, demonstrating a monodisperse suspension (Fig. S2).

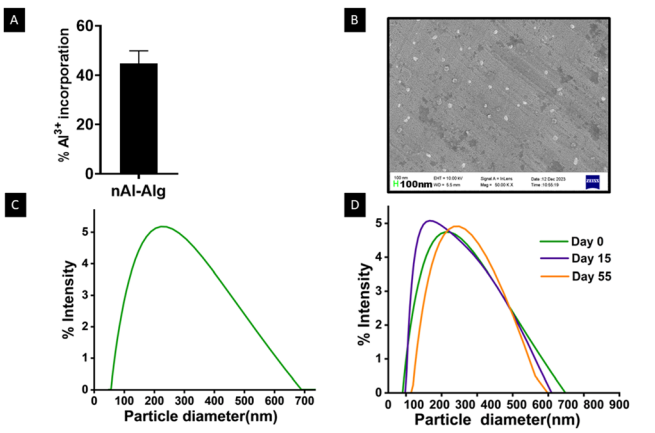

Fig. 1 (A) ICP data showing the average percentage of aluminium incorporated into three batches of nAl-Alg expressed as mean ± SEM. (B) FE-SEM image of nAl-Alg. (C) Intensity weighted particle distribution of nAl-Alg from DLS analysis. (D) Percentage intensity plot of nAl-Alg at different time intervals: day 0, day 15, and day 55.

The EDX spectrum of nAl-Alg was compared with that of sodium alginate to confirm the elemental composition of nAl-Alg. The spectrum confirmed the successful incorporation of aluminium (Al), as evidenced by the replacement of the sodium (Na) peak with the Al peak at 1.5 keV (Fig. 2A).

To gain further insight into the bonding between aluminium and alginate, the FTIR spectrum of nAl-Alg was compared with that of sodium alginate. The FTIR spectrum of sodium alginate in Fig. 2B exhibits various characteristic peaks corresponding to specific vibrational modes of functional groups. The peak at 3415 cm^{-1} signifies the stretching vibrations of hydroxyl groups (–OH), while the peak at 2922.1 cm^{-1} is attributed to the stretching vibrations of carbon–hydrogen bonds (C–H).[32] Similarly, the 1617.9 cm^{-1} and 1420 cm^{-1} peaks correspond to the carboxylate group's asymmetric and symmetric stretching vibrations (–COO).[33] Additionally, the peak at 1303.2 cm^{-1} indicates C–C–H deformation and the peak at 1085 cm^{-1} is observed due to the

© 2025 The Author(s). Published by the Royal Society of Chemistry

Open Access Article. Published on 19 September 2025. Downloaded on 4/28/2026 7:03:43 AM. This article is licensed under a Creative Commons Attribution 3.0 Unported Licence.

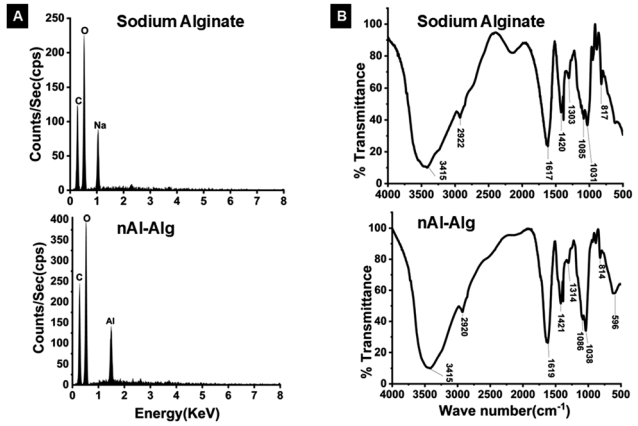

Fig. 2 (A) EDX spectra of sodium alginate and nAl-Alg. (B) FTIR spectra of sodium alginate and nAl-Alg.

stretching vibrations of C–O and C–C bonds within the pyranose ring.[34] The peak at 817.1 cm^{-1} represents a characteristic peak of mannuronic acid.[32,34,35] A comparison of the FTIR spectra of sodium alginate and nAl-Alg revealed no significant changes in the observed peaks, suggesting that the major functional groups remained unaltered upon crosslinking with aluminium. This lack of significant alterations can be attributed to the close ionic radii of Na^{+} and Al^{3+}, indicating that the ion exchange reaction minimally impacts the stretching vibrations of carboxylate groups (–COO–).[33]

ssNMR spectroscopy was utilized to further investigate the structural changes in nAl-Alg compared to sodium alginate. ^{1}H MAS-NMR spectra of sodium alginate and nAl-Alg exhibited peaks at −3.7 and −3.36 ppm, respectively (Fig. 3A). The peak width was reduced from 1.45 kHz in sodium alginate to 1.18 kHz in nAl-Alg. The observed shift in the peak can be attributed to the interaction of aluminium ions and the carboxyl groups of alginate. The overall peak pattern largely remains unchanged, suggesting that the basic structure of alginate remains the same. ^{13}C MAS-NMR reveals a broadening of the NMR peaks in nAl-Alg compared to sodium alginate, which may be attributed to variations in local environments, including conformational heterogeneity and differences in hydrogen bonding interactions (Fig. 3B).[36] Furthermore, ^{23}Na and ^{27}Al solid-state NMR spectroscopy were employed to characterize the compositional changes in alginate upon crosslinking with aluminium ions. As expected, the intensity of the sodium peak in the ^{23}Na MAS-NMR spectrum of nAl-Alg was significantly reduced compared to that of sodium alginate (Fig. S3A – SI), confirming the successful replacement of sodium ions with aluminum during the crosslinking process. The emergence of a prominent peak near −6.2 ppm in the ^{27}Al NMR spectrum of nAl-Alg, absent in the sodium alginate spectrum (Fig. S3B – SI), indicates the successful incorporation of aluminum within the alginate matrix.

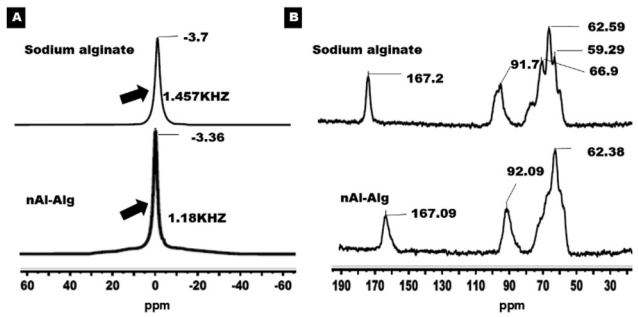

Fig. 3 (A) ^{1}H MAS-NMR spectra of sodium alginate and nAl-Alg. (B) ^{13}C MAS-NMR spectra of sodium alginate and nAl-Alg.

3.2 Bacterial endotoxin test of nAl-Alg

Prior to *in vitro* and *in vivo* studies, it is important to assess the endotoxin levels within the nAl-Alg formulation. The presence of endotoxins can alter the immune response elicited by the vaccine. While chromogenic assays generally offer higher sensitivity for endotoxin detection, potential interference from aluminum ions necessitated the use of the Limulus Amebocyte Lysate (LAL) assay in this study.[37] The LAL assay relies on the ability of LAL to form a gel-like clot in the presence of endotoxins. The nAl-Alg sample did not produce a clot, indicating the absence of detectable endotoxins within the limits of the assay sensitivity (0.05–0.1 EU mL^{-1}). The inhibitor tube (nAl-Alg + endotoxin standard) produced a clot, which indicates that no inhibitors for clot formation are present in nAl-Alg. The positive control exhibited clot formation, confirming the assay's functionality. The negative control, as expected, did not form a clot. Importantly, this study demonstrates that the nAl-Alg sample, within the sensitivity limits of the E-TOXATE™ LAL assay, is free from detectable endotoxins.

3.3. Cytocompatibility analysis of nAl-Alg

To evaluate the cytocompatibility of nAl-Alg, an MTT assay was conducted on the RAW 264.7 cell line. A macrophage cell line was selected because macrophages are among the first antigen presenting cells to respond to vaccine adjuvants initiating an immune response. Cell viability was assessed after a 48-hour incubation period with varying concentrations of nAl-Alg. As shown in Fig. 4A, the percentage of cell viability revealed that nAl-Alg concentrations up to 100 μg ml^{-1} did not cause any statistically significant change in viability compared to the untreated control. However, a reduction in cell viability to 59% was observed at 200 μg ml^{-1}. The results show the cytocompatibility of nAl-Alg up to a concentration of 100 μg ml^{-1}. This information is critical for assessing the safety and suitability of nAl-Alg for further preclinical studies.

3.4. Evaluation of nAl-Alg cellular uptake by lumogallion staining

Macrophage uptake of nAl-Alg was compared to that of Alhydrogel®, a clinically approved alum-based adjuvant, using the RAW 264.7 cell line. Lumogallion, a fluorescent probe that selectively binds aluminum was used to track intracellular aluminum distribution. Lumogallion exhibits fluorescence

© 2025 The Author(s). Published by the Royal Society of Chemistry

Open Access Article. Published on 19 September 2025. Downloaded on 4/28/2026 7:03:43 AM.
This article is licensed under a Creative Commons Attribution 3.0 Unported Licence.

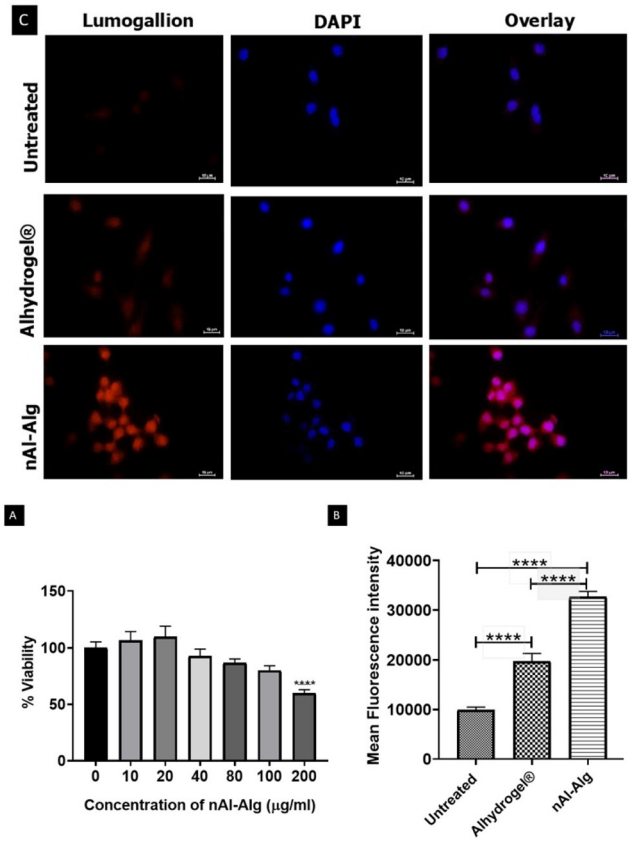

Fig. 4 (A) Percentage viability of RAW 264.7 following incubation with nAl-Alg at varying concentrations relative to untreated control cells. Data are presented as mean ± SEM (n = 9). The degree of significance is indicated where appropriate: $^{**}P < 0.01$ and $^{****}P < 0.0001$ (one-way ANOVA, Dunnett multiple comparison test). (B) Cell uptake study: mean fluorescence intensity of lumogallion for each group. Data are presented relative to untreated control as mean ± SEM, when n (number of cells) = 100, indicated where appropriate: $^{**}P < 0.01$ and $^{****}P < 0.0001$ (one-way ANOVA, Tukey's multiple comparison test). (C) Representative fluorescence images of lumogallion staining in RAW 264.7 macrophages.

emission between 520 nm and 650 nm when excited at 490 nm. In this study, RAW 264.7 cells were incubated with nAl-Alg and Alhydrogel® for 3 hours followed by lumogallion staining. Fig. 4B shows the mean fluorescence intensity (MFI) of 100 cells in each group, quantified using ImageJ software. The MFI of nAl-Alg (32 683.68 ± 1109) was significantly higher than that of control cells (9928.31 ± 573) and Alhydrogel®-treated (19 751.31 ± 1581.756) cells, indicating enhanced cellular uptake of nAl-Alg. This may be attributed to the smaller size of nAl-Alg compared to micron sized Alhydrogel. Fig. 4C depicts representative 60× fluorescence images of untreated cells, cells treated with Alhydrogel®, and cells treated with nAl-Alg. Previous studies have reported enhanced cellular uptake of nano-alum compared to alum, leading to improved antigen-specific immune responses.[38] Based on the observed enhanced cellular uptake of nAl-Alg compared to Alhydrogel®, we hypothesize that this may translate into improved antigen-specific immune responses *in vivo*.

3.5. *In vivo* toxicity studies

To assess the *in vivo* toxicity, two groups of C57BL/6 mice received nAl-Alg and saline on days 0, 5, and 10, according to the dosing schedule illustrated in Fig. 5A. 24 hours after the final dose (day 11), all animals were euthanised, and blood parameters of both saline-treated and nAl-Alg-treated animals were analysed. The evaluation involved parameters such as haemoglobin (Hb), red blood cell count (RBC), platelet count, and total white blood cell count (WBC), as depicted in Fig. 5B (i–iv). The figures indicate no significant difference between nAl-Alg-treated and saline-treated animals for any of these parameters. These findings suggest that nAl-Alg did not induce acute haematological toxicity within the tested time frame and dosage levels. Furthermore, the hepatic function was evaluated by analysing aspartate aminotransferase (AST) and alanine aminotransferase (ALT) levels, as shown in Fig. 5B (v and vi). Renal function was assessed through blood urea nitrogen (BUN) and creatinine tests, as illustrated in Fig. 5B(vii and viii). The results displayed no significant difference in concentrations between the treated and control groups, suggesting that nAl-Alg did not induce any detectable hepatic or renal toxicity at the administered dose. The absence of toxicity in blood parameters associated with the administered nAl-Alg dose supports further evaluation of its therapeutic potential in tumour models. To comprehensively assess nAl-Alg safety, hematoxylin and eosin staining of all major organs can be performed following vaccination as an additional evaluation of potential toxicity.

3.6. *In vivo* tumour model study

Furthermore, nAl-Alg was investigated for its efficacy as an adjuvant in therapeutic cancer vaccines using a subcutaneous B16-F10 mouse melanoma model. The B16-F10 lysate was used as the antigen for this study and was mixed with nAl-Alg to formulate the vaccine. Although tumor antigen loading within the nanomaterial is possible, we obtained a very low encapsulation efficiency (7.5–15.3%, Fig. S4) using bovine serum

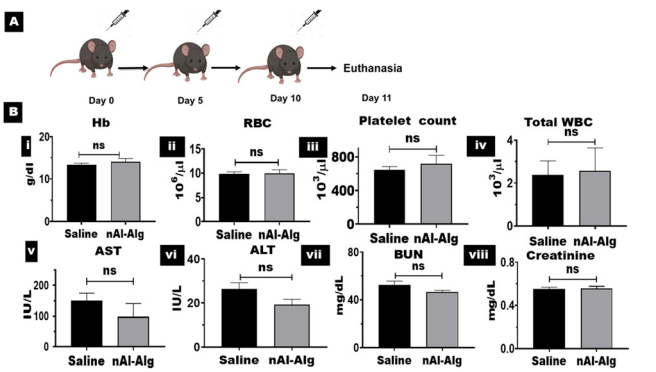

Fig. 5 (A) Immunization schedule for *in vivo* toxicity studies. (B) A comparison of different blood parameters – (i) Hb (ii) RBC (iii) Platelet Count (iv) Total WBC (v) AST (vi) ALT (vii) BUN (viii) Creatinine – of nAl-Alg treated animals with the saline-treated animals, as mean ± SEM, where n = 3. The degree of significance is indicated where appropriate: $^{*}P < 0.05$ and $^{***}P < 0.0005$ (Student's t-test).

© 2025 The Author(s). Published by the Royal Society of Chemistry

Open Access Article. Published on 19 September 2025. Downloaded on 4/28/2026 7:03:43 AM. This article is licensed under a Creative Commons Attribution 3.0 Unported Licence.

albumin as a model antigen; the methods and detailed results are discussed in section S4. Therefore, for this work, tumor antigens were mixed with nAl-Alg immediately prior to use.

The different groups tested for the anti-tumour study were (i) an untreated control group, (ii) a group treated with nAl-Alg alone, (iii) a group treated with tumour lysate alone, and (iv) a group treated with a combination of tumour lysate and nAl-Alg. In the tumour model study depicted in Fig. 6A, tumour measurements were taken from the 5th day following tumour induction. Animals were subcutaneously vaccinated on days 5, 10, and 15 post-tumor implantation. Euthanasia was performed after tumours reached a maximum size of 2 cm^3.

Notably, the group treated with a combination of tumour lysate and nAl-Alg exhibited a slower tumour growth rate compared to all other groups, as shown in Fig. 6B. This observation was further supported by Kaplan–Meier survival plots created for each group, as depicted in Fig. 6C. Median survival significantly increased from 17 days in the untreated control group to 24 and 23 days in groups treated with tumor lysate alone and nAl-Alg alone, respectively. Remarkably, the combination of tumor lysate and nAl-Alg extended median survival to 33 days, demonstrating a 94% increase compared to untreated controls. These results highlight the potential of nAl-Alg to augment the efficacy of tumor antigen-based vaccines by slowing the tumor growth rate and prolonging survival time in animal models. The observed increase in median survival time in the tumor lysate alone treated group is expected, as tumor lysate provides a complex mixture of tumor antigens that can stimulate antigen-specific immune responses.[39] The nAl-Alg alone treated group also exhibited reduced tumor growth and improved survival compared to the untreated control, likely due to a non-specific activation of the immune response. These findings align with those reported by Liu *et al.*, who observed similar tumor growth inhibition using silica nanoparticles.[40] The inclusion of alum plus antigen controls is highly relevant for a comprehensive evaluation of the present study. Therefore, subsequent investigations will incorporate these controls. Analysis of tumour-infiltrating $CD3e^+CD8a^+$ double positive cells revealed an increase in the nAl-Alg plus tumour lysate treated group (2.9 ± 0.54%) compared to the nAl-Alg alone (1.24 ± 0.59%), tumour lysate alone (0.59 ± 0.15%) and untreated control groups (0.33 ± 0.21%) (Fig. S5). These results indicate that the use of nAl-Alg as an adjuvant in therapeutic cancer vaccines enhances cytotoxic T cell infiltration within tumours, an essential mechanism for effective anti-tumour immunity. One limitation of this study is the absence of cytokine profiling following nAI-Alg treatment; future work will investigate the cytokine-mediated mechanisms in greater detail.

Previous studies have demonstrated the efficacy of aluminum-based nanoparticles as adjuvants in therapeutic cancer vaccines. For instance, aluminum oxide nanoparticles have shown superior tumor growth inhibition compared to alum in the H22 mouse hepatocellular carcinoma model.[25] A similar study utilizing aluminum-based layered double hydroxide as an adjuvant in a melanoma vaccine reported a 76% tumor suppression rate when administered *via* a combination of intravenous and subcutaneous routes.[41] Compared to alum-based adjuvants, which exhibit slow *in vivo* degradation,[27] alginate-based formulations, such as nAl-Alg, offer the potential for improved biodegradability and clearance.[28]

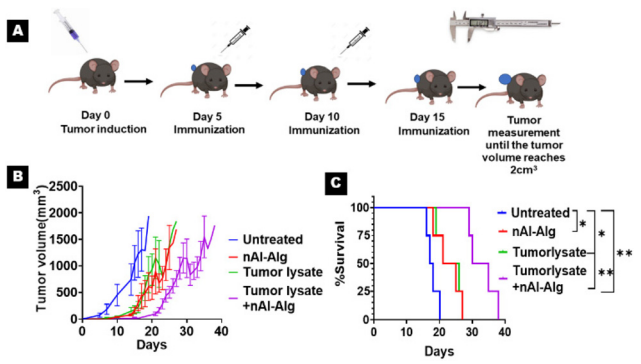

Fig. 6 (A) Schematic representation of the anti-tumor study in a subcutaneous mouse melanoma model. (B) Tumour volume of the respective groups in mm^3 (mean ± SEM). (C) Kaplan–Meir survival plot showing the survival curves of each group. Curve comparison was performed using the log-rank (Mantel–Cox) test. n = 4.

4. Conclusion

In conclusion, our study presents a promising strategy to enhance the efficacy of peptide-based therapeutic cancer vaccines using nAl-Alg as an adjuvant. DLS analysis confirmed that we optimised the synthesis parameters to achieve ~242 nm sized nAl-Alg. EDX and NMR spectra confirmed the successful incorporation of aluminium within nAl-Alg. FTIR spectroscopy revealed minimal alteration in functional groups upon crosslinking with aluminium. The cytocompatibility was confirmed through *in vitro* studies, ensuring its suitability for further investigation. Cellular uptake studies of nAl-Alg demonstrated significantly higher uptake of nAl-Alg compared to that of Alhydrogel®, a commercially available aluminium hydroxide adjuvant. This enhanced cellular uptake suggests the possibility for better antigen specific immune responses. Additionally, *in vivo* toxicity assessments revealed no adverse effects on haematological parameters, indicating the safety of nAl-Alg administration in animal models. The therapeutic efficacy of nAl-Alg as an adjuvant was demonstrated in the B16-F10 mouse melanoma model. Mice treated with a combination of nAl-Alg and the tumour antigen exhibited slower tumour growth and a prolonged median survival time of 33 days compared to 17 days in the untreated control group and 24 and 23 days in groups treated with tumor lysate alone and nAl-Alg alone, respectively. Overall, these results underscore the potential of nAl-Alg to enhance the immune response of therapeutic cancer vaccines against tumours.

© 2025 The Author(s). Published by the Royal Society of Chemistry

Open Access Article. Published on 19 September 2025. Downloaded on 4/28/2026 7:03:43 AM. This article is licensed under a Creative Commons Attribution 3.0 Unported Licence.

Conflicts of interest

There are no conflicts to declare.

Data availability

All data that support the findings of this study are available in the manuscript, supporting information (SI) and data repository (https://doi.org/10.17632/2h7rsmbv65.1). Supplementary information is available. See DOI: https://doi.org/10.1039/d5pm00111k.

Acknowledgements

The authors acknowledge financial support from the Department of Science and Technology (Inspire Faculty Project – DST/INSPIRE/04/2015/002761), India. M. M. T. P. thanks the Cochin University of Science and Technology for the Junior Research Fellowship. The authors thank Dr S. Prathapan, CUSAT, for his assistance in the analysis of NMR data. The authors acknowledge the support of the Department of Biotechnology, CUSAT from RUSA, FIST, and PURSE. Analytical techniques, including FTIR, EDX, and ICP-MS, were conducted at DST SAIF Cochin (CUSAT). FE-SEM analysis was performed at the Department of Physics, CUSAT. DLS analysis was conducted at the Central Instrumentation Facility of Bharata Mata College, Kochi. NMR analysis was done at the NMR facility, Centre for Material Characterization, NIT Calicut.

References

1 T. Fan, M. Zhang, J. Yang, Z. Zhu, W. Cao and C. Dong, Therapeutic Cancer Vaccines: Advancements, Challenges, and Prospects, *Signal Transduction Targeted Ther.*, 2023, **8**(1), 1–23, DOI: 10.1038/s41392-023-01674-3.

2 C. S. Shemesh, J. C. Hsu, I. Hosseini, B.-Q. Shen, A. Rotte, P. Twomey, S. Girish and B. Wu, Personalized Cancer Vaccines: Clinical Landscape, Challenges, and Opportunities, *Mol. Ther.*, 2021, **29**(2), 555–570, DOI: 10.1016/j.ymthe.2020.09.038.

3 S. Puth, V. Verma, S. H. Hong, W. Tan, S. E. Lee and J. H. Rhee, An All-in-One Adjuvanted Therapeutic Cancer Vaccine Targeting Dendritic Cell Cytosol Induces Long-Lived Tumor Suppression through NLRC4 Inflammasome Activation, *Biomaterials*, 2022, **286**, 121542, DOI: 10.1016/j.biomaterials.2022.121542.

4 J. Liu, M. Fu, M. Wang, D. Wan, Y. Wei and X. Wei, Cancer Vaccines as Promising Immuno-Therapeutics: Platforms and Current Progress, *J. Hematol. Oncol.*, 2022, **15**(1), 28, DOI: 10.1186/s13045-022-01247-x.

5 F. Garrido, T. Cabrera and N. Aptsiauri, "Hard" and "Soft" Lesions Underlying the HLA Class I Alterations in Cancer Cells: Implications for Immunotherapy, *Int. J. Cancer*, 2010, **127**(2), 249–256, DOI: 10.1002/ijc.25270.

6 R. E. Toes, R. Offringa, R. J. Blom, C. J. Melief and W. M. Kast, Peptide Vaccination Can Lead to Enhanced Tumor Growth through Specific T-Cell Tolerance Induction, *Proc. Natl. Acad. Sci. U. S. A.*, 1996, **93**(15), 7855–7860, DOI: 10.1073/pnas.93.15.7855.

7 W. G. Kim, B. Choi, H.-J. Yang, J.-A. Han, H. Jung, H. Cho, S. Kang and S. Y. Hong, Covalent Conjugation of Small-Molecule Adjuvants to Nanoparticles Induces Robust Cytotoxic T Cell Responses via DC Activation, *Bioconjugate Chem.*, 2016, **27**(9), 2007–2013, DOI: 10.1021/acs.bioconjchem.6b00277.

8 K. S. Korsholm, J. Hansen, K. Karlsen, J. Filskov, M. Mikkelsen, T. Lindenstrøm, S. T. Schmidt, P. Andersen and D. Christensen, Induction of CD8+ T-Cell Responses against Subunit Antigens by the Novel Cationic Liposomal CAF09 Adjuvant, *Vaccine*, 2014, **32**(31), 3927–3935, DOI: 10.1016/j.vaccine.2014.05.050.

9 W. T. Heng, H. X. Lim, K. O. Tan and C. L. Poh, Validation of Multi-Epitope Peptides Encapsulated in PLGA Nanoparticles Against Influenza A Virus, *Pharm. Res.*, 2023, **40**(8), 1999–2025, DOI: 10.1007/s11095-023-03540-x.

10 H. Li, S. Nookala and F. Re, Aluminum Hydroxide Adjuvants Activate Caspase-1 and Induce IL-1β and IL-18 Release1, *J. Immunol.*, 2007, **178**(8), 5271–5276, DOI: 10.4049/jimmunol.178.8.5271.

11 J. L. Grun and P. H. Maurer, Different T Helper Cell Subsets Elicited in Mice Utilizing Two Different Adjuvant Vehicles: The Role of Endogenous Interleukin 1 in Proliferative Responses, *Cell. Immunol.*, 1989, **121**(1), 134–145, DOI: 10.1016/0008-8749(89)90011-7.

12 S. Awate, L. A. Babiuk and G. Mutwiri, Mechanisms of Action of Adjuvants, *Front. Immunol.*, 2013, **4**, 114, DOI: 10.3389/fimmu.2013.00114.

13 H. Khong and W. W. Overwijk, Adjuvants for Peptide-Based Cancer Vaccines, *J. Immunother. Cancer*, 2016, **4**(1), 56, DOI: 10.1186/s40425-016-0160-y.

14 L. A. J. Feather, V. Nadella, E. Kastner, Y. Perrie, A. C. Hilton and A. Devitt, Development of a Rapid in Vitro Pre-Screen for Distinguishing Effective Liposome-Adjuvant Delivery Systems, *Sci. Rep.*, 2022, **12**(1), 12448, DOI: 10.1038/s41598-022-14449-7.

15 H. R. Nouri, A. Varasteh, M. R. Jaafari, J. M. Davies and M. Sankian, Induction of a Th1 Immune Response and Suppression of IgE via Immunotherapy with a Recombinant Hybrid Molecule Encapsulated in Liposome–Protamine–DNA Nanoparticles in a Model of Experimental Allergy, *Immunol. Res.*, 2015, **62**(3), 280–291, DOI: 10.1007/s12026-015-8659-8.

16 L. Sercombe, T. Veerati, F. Moheimani, S. Y. Wu, A. K. Sood and S. Hua, Advances and Challenges of Liposome Assisted Drug Delivery, *Front. Pharmacol.*, 2015, **6**, 286, DOI: 10.3389/fphar.2015.00286.

17 Y. Perrie, E. Kastner, S. Khadke, C. B. Roces and P. Stone, Manufacturing Methods for Liposome Adjuvants, *Methods Mol. Biol.*, 2017, **1494**, 127–144, DOI: 10.1007/978-1-4939-6445-1_9.

© 2025 The Author(s). Published by the Royal Society of Chemistry

Open Access Article. Published on 19 September 2025. Downloaded on 4/28/2026 7:03:43 AM. This article is licensed under a Creative Commons Attribution 3.0 Unported Licence.

18 S. Farfán-Castro, M. J. García-Soto, L. Betancourt-Mendiola, J. Cervantes, R. Segura, O. González-Ortega and S. Rosales-Mendoza, Synthesis and Evaluation of Gold Nanoparticles Conjugated with Five Antigenic Peptides Derived from the Spike Protein of SARS-CoV-2 for Vaccine Development, *Front. Nanotechnol.*, 2024, **6**, 1335346, DOI: 10.3389/fnano.2024.1335346.

19 B. G. Cha, J. H. Jeong and J. Kim, Large Pore Mesoporous Silica Nanoparticles Enabling Co-Delivery of High Amounts of Protein Antigen and Toll-like Receptor 9 Agonist for Enhanced Cancer Vaccine Efficacy, *ACS Cent. Sci.*, 2018, **4**, 484–492, DOI: 10.1021/acscentsci.8b00035.

20 V. Durán, H. Yasar, J. Becker, D. Thiyagarajan, B. Loretz, U. Kalinke and C-M. Lehr, Preferential Uptake of Chitosan-Coated PLGA Nanoparticles by Primary Human Antigen Presenting Cells, *Nanomedicine*, 2019, **21**, 102073, DOI: 10.1016/j.nano.2019.102073.

21 S.-Y. Kim, Y.-W. Noh, T. H. Kang, J.-E. Kim, S. Kim, S. H. Um, D.-B. Oh, Y.-M. Park and Y. T. Lim, Synthetic Vaccine Nanoparticles Target to Lymph Node Triggering Enhanced Innate and Adaptive Antitumor Immunity, *Biomaterials*, 2017, **130**, 56–66, DOI: 10.1016/j.biomaterials.2017.03.034.

22 S. M. Moghimi, A. E. Hawley, N. M. Christy, T. Gray, L. Illum and S. S. Davis, Surface engineered nanospheres with enhanced drainage into lymphatics and uptake by macrophages of the regional lymph nodes, *FEBS Lett.*, 1994, **344**, 25–30, DOI: 10.1016/0014-5793(94)00351-3.

23 C. Song, Y.-W. Noh and Y. T. Lim, Polymer Nanoparticles for Cross-Presentation of Exogenous Antigens and Enhanced Cytotoxic T-Lymphocyte Immune Response, *Int. J. Nanomed.*, 2016, **11**, 3753–3764, DOI: 10.2147/IJN.S110796.

24 H. Dong, Z. F. Wen, L. Chen, N. Zhou, H. Liu, S. Dong, H. Hu and Y. Mou, Polyethyleneimine Modification of Aluminum Hydroxide Nanoparticle Enhances Antigen Transportation and Cross-Presentation of Dendritic Cells, *Int. J. Nanomed.*, 2018, **13**, 3353–3365, DOI: 10.2147/IJN.S164097.

25 Z. Sun, W. Wang, R. Wang, J. Duan, Y. Hu, J. Ma, J. Zhou, S. Xie, X. Lu, Z. Zhu, S. Chen, Y. Zhao, H. Xu, C. Wang and X.-D. Yang, Aluminum Nanoparticles Enhance Anticancer Immune Response Induced by Tumor Cell Vaccine, *Cancer Nanotechnol.*, 2010, **1**(1–6), 63–69, DOI: 10.1007/s12645-010-0001-5.

26 M. T. Orr, A. P. Khandhar, E. Seydoux, H. Liang, E. Gage, T. Mikasa, E. L. Beebe, N. D. Rintala, K. H. Persson, A. Ahniyaz, D. Carter, S. G. Reed and C. B. Fox, Reprogramming the Adjuvant Properties of Aluminum Oxyhydroxide with Nanoparticle Technology, *npj Vaccines*, 2019, **4**, 1, DOI: 10.1038/s41541-018-0094-0.

27 R. K Gherardi, M. Coquet, P. Cherin, L. Belec, P. Moretto, P. A. Dreyfus, J. F. Pellissier, P. Chariot and F. J. Authier, Macrophagic Myofasciitis Lesions Assess Long-term Persistence of Vaccine-derived Aluminium Hydroxide in Muscle, *Brain*, 2001, **124**, 1821–1831, DOI: 10.1093/brain/124.9.1821.

28 J. Sun and H. Tan, Alginate-Based Biomaterials for Regenerative Medicine Applications, *Materials*, 2013, **6**(4), 1285–1309, DOI: 10.3390/ma6041285.

29 F. Dobakhti, T. Naghibi, M. Taghikhani, S. Ajdary, A. Rafinejad, K. Bayati, S. Rafiei and M. Rafiee-Tehrani, Adjuvanticity Effect of Sodium Alginate on Subcutaneously Injected BCG in BALB/c Mice, *Microbes Infect.*, 2009, **11**(2), 296–301, DOI: 10.1016/j.micinf.2008.12.003.

30 A. Unnikrishnan, M. Menon, K. G. Gopika, R. E. Sam, M. Koyakutty and A. Ashokan, Engineered Polymer-Based Scaffold as an Implantable Therapeutic Vaccine against Melanoma, *J. Appl. Polym. Sci.*, 2024, **141**, e55032, DOI: 10.1002/app.55032.

31 S. K. Filippov, R. Khusnutdinov, A. Murmiliuk, W. Inam, L. Ya. Zakharova, H. Zhang and V. V. Khutoryanskiy, Dynamic Light Scattering and Transmission Electron Microscopy in Drug Delivery: A Roadmap for Correct Characterization of Nanoparticles and Interpretation of Results, *Mater. Horiz.*, 2023, **10**(12), 5354–5370, DOI: 10.1039/D3MH00717K.

32 A. S. El-Houssiny, A. A. Ward, D. M. Mostafa, S. L. Abd-El-Messieh, K. N. Abdel-Nour, M. M. Darwish and W. A. Khalil, Drug–Polymer Interaction between Glucosamine Sulfate and Alginate Nanoparticles: FTIR, DSC and Dielectric Spectroscopy Studies, *Adv. Nat. Sci.: Nanosci. Nanotechnol.*, 2016, **7**(2), 025014, DOI: 10.1088/2043-6262/7/2/025014.

33 Q. Zhou, X. Lin, B. Li and X. Luo, Fluoride Adsorption from Aqueous Solution by Aluminum Alginate Particles Prepared via Electrostatic Spinning Device, *Chem. Eng. J.*, 2014, **256**, 306–315, DOI: 10.1016/j.cej.2014.06.101.

34 D. Leal, B. Matsuhiro, M. Rossi and F. Caruso, FT-IR, Spectra of Alginic Acid Block Fractions in Three Species of Brown Seaweeds, *Carbohydr. Res.*, 2008, **343**(2), 308–316, DOI: 10.1016/j.carres.2007.10.016.

35 N. P. Chandía, B. Matsuhiro and A. E. Vásquez, Alginic Acids in Lessonia Trabeculata: Characterization by Formic Acid Hydrolysis and FT-IR Spectroscopy, *Carbohydr. Polym.*, 2001, **46**(1), 81–87, DOI: 10.1016/S0144-8617(00)00286-1.

36 J. Brus, M. Urbanova, J. Czernek, M. Pavelkova, K. Kubova, J. Vyslouzil, S. Abbrent, R. Konefal, J. Horský, D. Vetchy, J. Vysloužil and P. Kulich, Structure and Dynamics of Alginate Gels Cross-Linked by Polyvalent Ions Probed via Solid State NMR Spectroscopy, *Biomacromolecules*, 2017, **18**, 2478–2488, DOI: 10.1021/acs.biomac.7b00627.

37 C.-Y. Park, S.-H. Jung, J.-P. Bak, S.-S. Lee and D.-K. Rhee, Comparison of the Rabbit Pyrogen Test and Limulus Amoebocyte Lysate (LAL) Assay for Endotoxin in Hepatitis B Vaccines and the Effect of Aluminum Hydroxide, *Biologicals*, 2005, **33**(3), 145–151, DOI: 10.1016/j.biologicals.2005.04.002.

38 B. Sun, Z. Ji, Y.-P. Liao, M. Wang, X. Wang, J. Dong, C. H. Chang, R. Li, H. Zhang, A. E. Nel and T. Xia, Engineering an Effective Immune Adjuvant by Designed Control of Shape and Crystallinity of Aluminum

Open Access Article. Published on 19 September 2025. Downloaded on 4/28/2026 7:03:43 AM.
This article is licensed under a Creative Commons Attribution 3.0 Unported Licence.

Oxyhydroxide Nanoparticles, *ACS Nano*, 2013, **7**(12), 10834–10849, DOI: 10.1021/nn404211j.

39 F. E. González, A. Gleisner, F. Falcón-Beas, F. Osorio, M. N. López and F. Salazar-Onfray, Tumor Cell Lysates as Immunogenic Sources for Cancer Vaccine Design, *Hum. Vaccines Immunother.*, 2015, **10**(11), 3261–3269, DOI: 10.4161/21645515.2014.982996.

40 Q. Liu, Y. Zhou, M. Li, L. Zhao, J. Ren, D. Li, Z. Tan, K. Wang, H. Li, M. Hussain, L. Zhang, G. Shen, J. Zhu and J. Tao, Polyethylenimine Hybrid Thin-Shell Hollow Mesoporous Silica Nanoparticles as Vaccine Self-Adjuvants for Cancer Immunotherapy, *ACS Appl. Mater. Interfaces*, 2019, **11**(51), 47798–47809, DOI: 10.1021/acsami.9b19446.

41 L. Zhang, X. Sun, Y. Jia, X. Liu, M. Dong, Z. P. Xu and R. Liu, Nanovaccine's Rapid Induction of Anti-Tumor Immunity Significantly Improves Malignant Cancer Immunotherapy, *Nano Today*, 2020, **35**, 100923, DOI: 10.1016/j.nantod.2020.100923.

© 2025 The Author(s). Published by the Royal Society of Chemistry